Published on 13 December 2013. Downloaded by Memorial University of Newfoundland on 22/06/2014 16:08:23.

Lab on a Chip

PAPER

View Article Online
View Journal | View Issue

Large scale arrays of tunable microlenses†

Cite this: *Lab Chip*, 2014, **14**, 1330

Atul Varshney,*[a] Smita Gohil,[a] Somayeh Khajehpour Tadavani,[b] Anand Yethiraj,*[b] S. Bhattacharya[a] and Shankar Ghosh*[a]

Received 14th October 2013,
Accepted 12th December 2013

DOI: 10.1039/c3lc51170g

www.rsc.org/loc

We demonstrate a simple and robust method to produce large 2-dimensional and quasi-3-dimensional arrays of tunable liquid microlenses using a time varying external electric field as the only control parameter. With increasing frequency, the shape of the individual lensing elements (~40 μm in diameter) evolves from an oblate (lentil shaped) to a prolate (egg shaped) spheroid, thereby making the focal length a tunable quantity. Moreover, such microlenses can be spatially localized in desired configurations by patterning the electrode. This system has the advantage that it provides a large dynamic range of shape deformation (with a response time of ~30 ms for the whole range of deformation), which is useful in designing adaptive optics.

Introduction

Arrays of microlenses with focal lengths that can be dynamically controlled are useful for a large number of device applications that require real time control of the optical components. In most realizations, these lenses are made of liquid droplets of sizes ranging from a few 100 μm to a few mm.[1–3] The shape of these droplets and thereby their focusing property is manipulated in microfluidic devices, in the presence of stimuli such as temperature,[4,5] hydrostatic pressure,[6–8] an electric field,[1,3,9–11] pH,[5] or light.[12]

In the literature, the percentage change in focal length that has been achieved for large size droplets (~300 μm) is about 40% and the typical response time is of the order of tens of ms.[1] In most of these systems, different stimuli are used to produce and to actuate the microlens arrays. For example, in microfluidic devices, flow-induced shear stresses produce the droplet array while hydrostatic pressure is used to actuate it.[6,7,13,14] Pressure control[7] achieves a large focal length range, but it cannot be integrated as easily into an optical device as electric field-based control. Droplet manipulation based on electrowetting, where an electric field is a stimulus, is very attractive: the voltages are small, and the droplet lenses can be made flat, so the change in focal length can be appreciable. But it is very difficult to use electrowetting to make symmetric biconvex and composite lenses with controllable shapes, and in addition, there are inherent problems associated with liquid electrolysis[10] and contact-angle hysteresis.[11] Microlens arrays are useful in diverse applications where enhanced light collection is required at low cost. For example, microlens arrays have been utilized to increase the effective quantum efficiency of high-speed cameras by focusing light onto a pixel that would otherwise fall on the dead space between pixels.[15] Multi-pinhole confocal microscopes (such as swept field or spinning disk confocal microscopes[16]) use microlens arrays where the lens diameter and separation is 25–50 μm. Here, the purpose of the microlens array is to increase the effective area of the sample scanned without a corresponding decrease in the scan speed. An array of microlenses where the Z focusing could be field controllable, would be attractive.

In this paper, we demonstrate the working of a self-organized frequency-tunable liquid microlens array, which uses a time-varying electric field as a single stimulus in order to both produce and actuate 2-dimensional and quasi-3-dimensional configurations of liquid droplets. The droplet microlenses generated in this way have a cross-sectional diameter of ~40 μm and can be positioned into arrays with a separation of ~60 μm. The 2D biconvex droplets allow focal length control from 90 to 120 μm at a numerical aperture of 0.2 and the realization of quasi-3D configurations is a first step in control towards composite lenses.

Experimental methods

The experimental set-up, shown in Fig. 1, consists of two parallel ITO coated glass coverslips (thickness = 150 μm) separated by two glass spacers of thickness d ~ 120 μm. A drop of silicone oil (Dow Corning, dielectric constant (ε_{in}) = 2.75, conductivity (σ_{in}) = 3.6 × 10^{-10} S m^{-1} and viscosity (η_{in}) = 0.38 Pa s) is suspended in immersion oil (Immersol 518F, Zeiss, ε_{ex} = 4.66, σ_{ex} = 4.7 × 10^{-10} S m^{-1} and η_{ex} = 0.36 Pa s),

[a] Department of Condensed Matter Physics and Materials Science, Tata Institute of Fundamental Research, Homi Bhabha Road, Mumbai 400-005, India. E-mail: atulv@tifr.res.in, sghosh@tifr.res.in
[b] Department of Physics and Physical Oceanography, Memorial University, St. John's, Newfoundland and Labrador, Canada, A1B 3X7. E-mail: ayethiraj@mun.ca

† Electronic supplementary information (ESI) available. See DOI: 10.1039/c3lc51170g

This journal is © The Royal Society of Chemistry 2014

Published on 13 December 2013. Downloaded by Memorial University of Newfoundland on 22/06/2014 16:08:23.

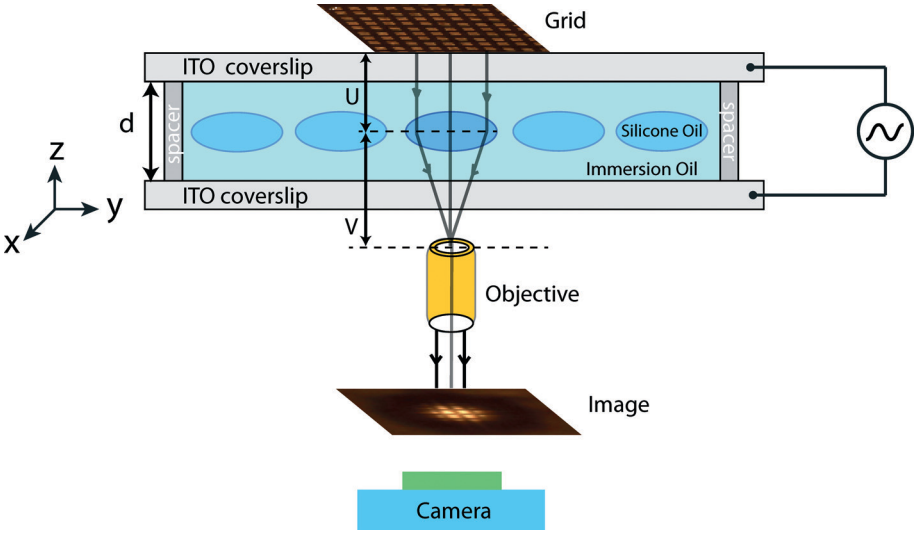

Fig. 1 Schematic of the experimental setup and ray diagram for the focusing of a single droplet lens. The spacing between the electrodes is *d*. *U* and *V* are the distances between the drop plane and the grid (object) plane, and the drop plane and the image plane, respectively.

which fills the inside of the system. The immersion oil mainly contains di-(TCD-methylol)-adipate (~70% volume) and benzylbenzoate (~20% volume). The system is sealed with ultraviolet curing adhesive on all sides to prevent any liquid leakage. A sinusoidal a.c. voltage (Trek 10/10B-HS), amplitude: 0–10 kV, frequency: 0–19 kHz, is applied between the planar electrodes, so that the electric field is perpendicular to the plane of the electrodes (which is also the image plane). The system is imaged directly *via* a bright field microscope (Nikon TE300) and using a (4×–40× air) microscope objective. A CCD camera (UK 1157 from EHD imaging GmbH) attached to the microscope captures the system image. A grid of 8 μm × 8 μm squares, made on a gold film by e-beam lithography, is used as an object to image through the drop. A ray diagram of the focusing of the grid through a single drop is shown schematically in Fig. 1: *U* is the distance between the grid (object) plane and the drop plane, and *V* is the distance between the drop plane and the image plane.

Results and discussion

Drops with a frequency-tunable focal length

The control of the focal length (f) of a tunable microlens is demonstrated in Fig. 2a, which shows a sequence of

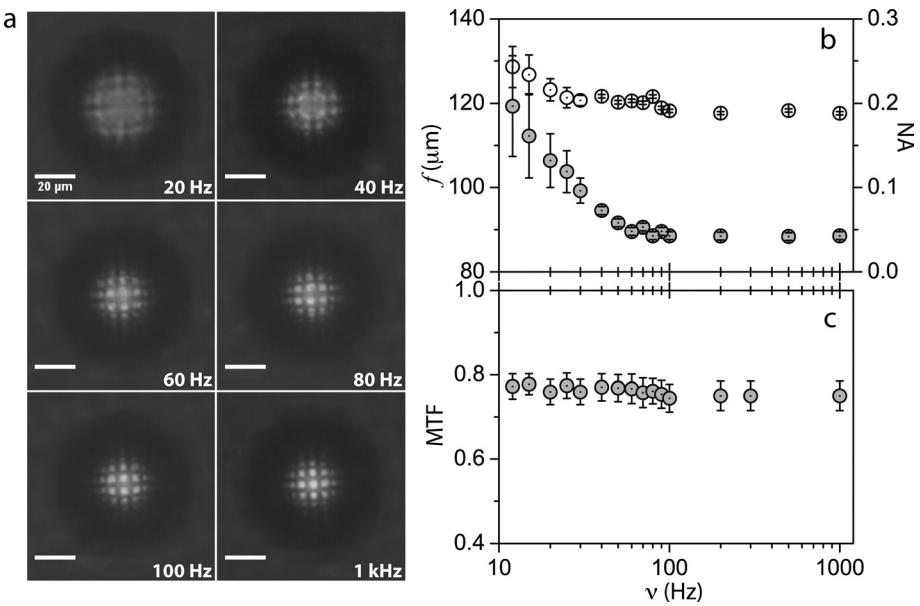

Fig. 2 A frequency-tunable focal length. (a) A sequence of micrographs obtained at different frequencies shows the focusing of the grid through the drop. (b) At each frequency, the focal length (f) can be measured by bringing the image of the grid into focus by manually refocusing the microscope objective to vary *V*, *i.e.*, the distance from the drop plane to the image plane. The graph shows the variation of focal length (filled circles) and numerical aperture (NA, open circles) with frequency, ν, at E = 10 V μm^{-1}. (c) Variation of the modulation transfer function (MTF) of the microlens at focus with ν.

Published on 13 December 2013. Downloaded by Memorial University of Newfoundland on 22/06/2014 16:08:23.

micrographs of a droplet of diameter $2a$ = 40 μm driven at different frequencies. An underlying grid of 8 μm × 8 μm squares is imaged through the droplet. The grid is highly defocused at 20 Hz and comes into focus as the frequency is increased to ν = 100 Hz. Above 100 Hz, no significant change is observed in the focused image of the grid. This control of focus arises due to a frequency driven transition[17] from a lower-frequency electrohydrodynamic regime, where tangential stresses compress the droplets into oblate (lentil shaped) spheroids, to a high-frequency dipolar regime, where the normal electric stresses elongate the droplets along the field direction into prolate (egg shaped) spheroids. Further details about the working principle are provided in what follows. The focal length of the droplet lens is determined using the expression $f = UV/(U + V)$.[18]

We measure V at each frequency by manually adjusting the objective to get the image of the grid through the droplet in the focal plane of the objective. The typical value of U is ~300 μm and V ranges from 120 (at 1 kHz) to 200 μm (at 12 Hz). The ray diagram of lens focusing is shown schematically in Fig. 1. The variation of f as a function of frequency (ν) is shown in Fig. 2b. The focal length decreases with increasing frequency up to 100 Hz and then saturates thereafter. The numerical aperture (NA) = $n \tan^{-1}(a/2f)$,[18] where n is the refractive index of immersion oil (n = 1.52), and the NA of the microlens varies from 0.19 to 0.25 in the frequency range of 12 Hz to 1 kHz, as shown in Fig. 2b. The performance of the microlens is characterized by computing the modulation or contrast transfer function from the intensity distribution across the diameter of the microlens at focus. The modulation transfer function (MTF) of the lens is defined as MTF = M_i/M_o, where image modulation (M_i) = $(I_{max} - I_{min})/(I_{max} + I_{min})$, I_{max} and I_{min} are maximum and minimum intensities in the image, respectively, and M_o is the object modulation similarly derived from the maximum and minimum intensities of the object.[19] The variation of the MTF of the microlens at focus with frequency (ν) is shown in Fig. 2c. The optical property of the microlens array is characterized by the f-number (= $f/2a$). A histogram of the f-numbers is displayed in Fig. S2 of the ESI.†

The voltages are large (~1 kV per 100 μm), but the applied frequency range over which the focal length changes appreciably is between 15 Hz to 100 Hz. In addition, the currents are very small, much less than 100 μA. Therefore, low-power amplifiers with small bandwidths are adequate.

Electrohydrodynamics-based working principle

The device works on the principle that a dielectric liquid drop suspended in a "leaky dielectric" medium undergoes shape deformation in the presence of an electric field.[20–23] In the case of leaky dielectrics, charge accumulates at the two fluid interface to conserve the current. The action of the electric field on the surface charge gives rise to tangential stresses, which cause circulatory flows within and outside the drop, which lead to shape deformation. In the presence of an electric field, an initially spherical drop of radius a is deformed into a spheroid with dimensions $d_{||}$ and $d_{\perp}$, and a dimensionless deformation $D = (d_{||} - d_{\perp})/(d_{||} + d_{\perp})$. The deformation ($D$) of a drop of radius a in a steady d.c. field (E) is given by[20] $D/aE^2 = 9\varepsilon_0\varepsilon_{ex}\,\Phi/16\gamma S(2 + R)^2$, where ε_0 is the free space permittivity, γ is the interfacial tension, $\Phi = S(R^2 + 1) - 2 + 3(RS - 1)(2M + 3)/(5M + 5)$, $R = \sigma_{in}/\sigma_{ex}$, $S = \varepsilon_{ex}/\varepsilon_{in}$, and $M = \eta_{in}/\eta_{ex}$. Therefore, the shape of the drop in a steady field can either be prolate ($D > 0$, major axis parallel to the field direction), oblate ($D < 0$, major axis perpendicular to the field direction), or spherical (D = 0) for a given set of material constants (such as conductivity, dielectric constant and viscosity).[20,21,23]

This frequency dependence may be understood by considering Torza *et al.*'s extension of the leaky dielectric model to an oscillatory (a.c.) electric field and calculating the electric stress on a single drop.[24] The stress, at a constant field amplitude and for a given material's constants, is a function of the frequency of the applied field and the angle between the radial vector of the drop and the field direction. The total stress is a sum of the normal and tangential stresses, which include both dipolar and hydrodynamic contributions, and each has two parts; time independent and time dependent. The time independent part of the normal stress gives rise to a steady droplet shape while the time dependent component gives rise to the shape oscillation. The time independent component of the stress is calculated from the expression derived by Torza *et al.*[24] and adapted from the ESI† of Varshney *et al.*[17] The expressions for the normal ($F_{r\nu}$) and transverse ($F_{\theta\nu}$) stresses at the droplet surface, in non-dimensional form, are

$$F_r \equiv \frac{F_{r\nu}}{\epsilon_0\epsilon_{ex}E^2} = \frac{9}{4}\frac{[(R^2 - 2SR^2 + 1) + \tau^2\omega^2(S-1)^2]\cos^2\theta + (S-1)(R^2 + \tau^2\omega^2)}{(2R+1)^2 + \tau^2\omega^2(S+2)^2} \quad (1)$$

$$F_\theta \equiv \frac{F_{\theta\nu}}{\epsilon_0\epsilon_{ex}E^2} = \frac{9}{2}\left[\frac{R(RS-1)}{(2R+1)^2 + \tau^2\omega^2(S+2)^2}\right]\cos\theta\sin\theta \quad (2)$$

where $\omega = 2\pi\nu$, $R = \sigma_{ex}/\sigma_{in}$, $S = \varepsilon_{in}/\varepsilon_{ex}$, $\tau = \varepsilon_0\varepsilon_{ex}/\sigma_{in}$ and θ is the angle between the radius vector and the field direction. Thus, the total stress on the droplet is $F = \sqrt{F_r^2 + F_\theta^2}$ and it decreases with increasing frequency, as shown in Fig. 3a. The angular dependency of the normal stress is shown in Fig. 3b. The resulting frequency-dependent drop shape at E = 5 V μm^{-1} is shown in Fig. 3c. The detailed dependence, on both frequency and field intensity (E^2), of the drop anisotropy is shown in Fig. S1 of ESI.†

 This journal is © The Royal Society of Chemistry 2014

Published on 13 December 2013. Downloaded by Memorial University of Newfoundland on 22/06/2014 16:08:23.

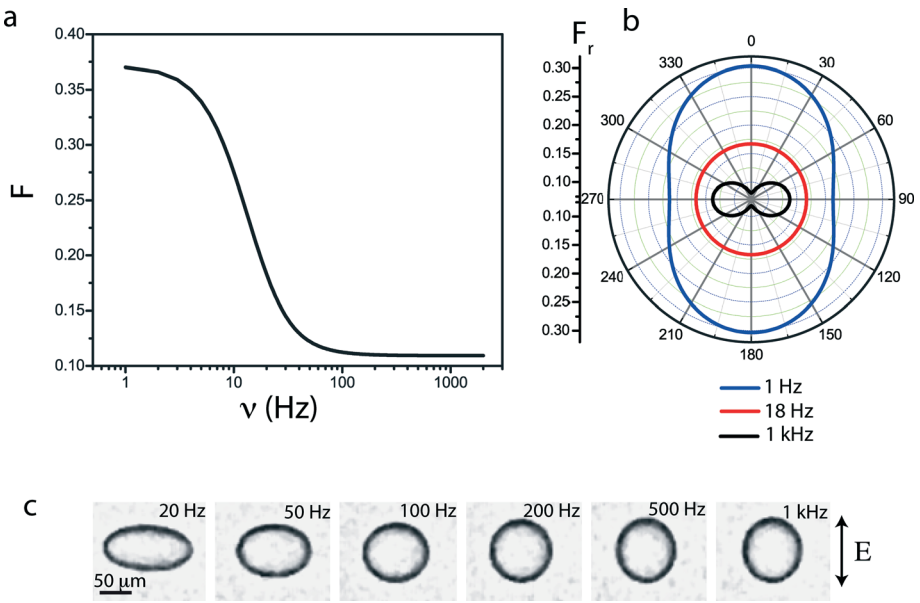

Fig. 3 Electrohydrodynamics-driven stresses on a liquid drop. (a) The variation of the total stress (calculated from the expressions given in ref. 24) on the drop with the applied frequency, ν. (b) The radial plot of the magnitude of the normal component of the stress for three frequencies; the direction is radially inward. For low frequencies, the inward force at the pole exceeds that at the equator and the resulting shape of the drop is oblate. For high frequencies, the inward force at the equator exceeds that at the pole and the resulting shape of the drop is prolate. At a crossover frequency, the radial plot is circular, and the drop remains spherical because the normal stress is isotropic. (c) The resulting frequency-dependent drop shape at E = 5 V μm^{-1}.

In the observations reported here, the scaled deformation D/a changes significantly up to ν_c and above the variation of D/a becomes small. This manifests itself as a strong frequency dependence of the focal length below ν_c, but a significantly weaker dependence above ν_c. At high frequencies, the normal stress at the pole (direction being radially inwards) is smaller than at the equator and the result is a prolate spheroidal droplet. At an intermediate frequency ν_c, the stresses at the pole and the equator get balanced giving rise to a spherical drop.[24] At low frequencies, the main contribution to the electric stress comes from the tangential component, which exceeds the interfacial tension of the droplet and therefore, gives rise to the breakup of droplets (Fig. 4a) into smaller droplets with a broad size distribution (Fig. 4b–c).[25] The shape of the droplets and thereby their focusing property is thus controlled by simply changing the frequency of the imposed electric field. The protocol of making nearly monodisperse droplets and their arrangement in an array is discussed next.

A self-assembly route for 2D and quasi-3D microlens arrays

While the results shown above discuss primarily the lensing produced by a single droplet, our methods are, in fact, capable of systematically producing very large (centimeter-scale) arrays of relatively monodisperse (~10% polydispersity) droplets (see Fig. S2 of ESI†). Moreover, while the drops themselves are convex three-dimensional (3D) objects, the droplet configurations are either two-dimensional or (quasi)-three-dimensional depending on the exact route of formation: this is described next.

Initially, a d.c. electric field of amplitude E = 10 V μm^{-1} is applied across the device. This causes the large silicone oil drop (Fig. 4a) to break into smaller size droplets (Fig. 4b).

In order to obtain 2D or quasi-3D arrays of droplets, we apply a very low frequency field (ν = 0.01 Hz, E = 10 V μm^{-1}) to the system (Fig. 4c). At this frequency, the droplets undergo convective rolls and periodically migrate between the two electrodes. When the field crosses zero, the droplets are found to come into a plane (Fig. 4d) close to the electrode. At this point of the cycle, the frequency is then raised to 1 Hz where a size-selective in-plane break-up of the large size droplets takes place due to the large tangential stresses. Thus, the droplet size distribution narrows down (Fig. 4e). The system is then quenched to 1 kHz and we obtain a 2D array of droplets (Fig. 4f). At ν = 1 kHz, the interaction between the droplets is mainly due to the dipolar field.

To obtain a quasi-3D array, we again increased the frequency from 0.01 Hz (Fig. 4g) to 1 Hz (Fig. 4h), *i.e.*, from the state where the system of droplets is migrating from one electrode to the other, to the state where size-selective droplet breakup occurs. We found that when the frequency switch to 1 Hz is made at a point in the cycle when the magnitude of the electric field is increasing, the droplets are distributed homogeneously across the system volume. As before, the 1 Hz field has the effect of narrowing the size distribution (Fig. 4h). Next, we quenched the system at 1 kHz, as shown in Fig. 4i. Remarkably, the droplets have now arranged themselves into two planes away from the electrode surface and symmetrically about the mid-plane between the electrodes. In the example shown (Fig. 4i), the droplets have an in-plane

Published on 13 December 2013. Downloaded by Memorial University of Newfoundland on 22/06/2014 16:08:23.

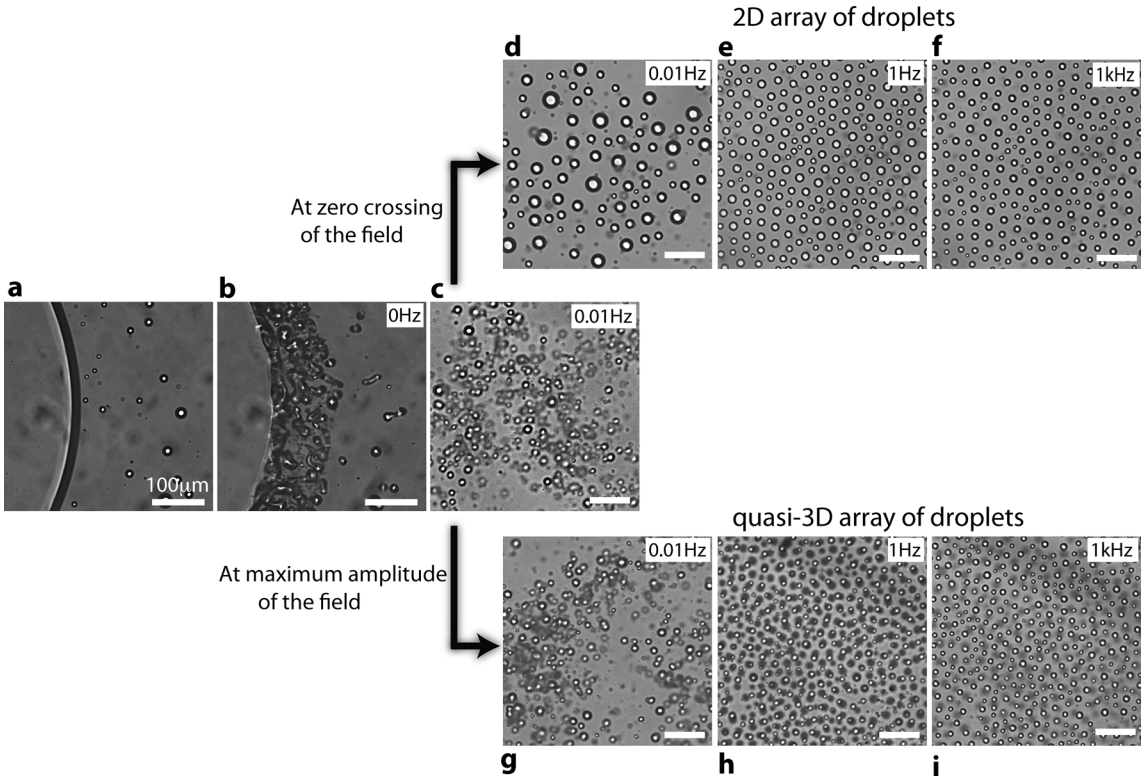

Fig. 4 Self-assembly route for 2D and 3D microlens arrays. (a) Interface between silicone oil (left) and immersion oil (right) at zero field. (b) Break-up of the silicone drop at E = 10 V μm^{-1}, ν = 0 Hz. (c) Snapshot of the convective flows at E = 10 V μm^{-1}, ν = 0.01 Hz. (*c* → *d* → *e* → *f*) A sequence of micrographs showing the route to obtain a 2D array. (*c* → *g* → *h* → *i*) A sequence of micrographs showing the route to obtain a quasi-3D array. For both sequences, the amplitude of the applied a.c. electric field is maintained at E = 10 V μm^{-1}. The respective frequencies are shown in the micrographs. Scale bars, 100 μm.

spacing of about 30 μm. The separation between the droplet plane and the electrode surface arises from the balance between the static electrostatic interaction between the electrode and the droplets, and the dipolar interaction among the droplets in a plane. The angular correlations of the droplets within a plane (see Fig. S2 of the ESI†) shows an interesting dependence on the separation between the electrodes: an increase in separation decreases the correlation between the planes, and increases in-plane order. The robustness of the protocol and the reproducibility of the arrays were tested by repeating the experiment more than ten times. Moreover, the arrays remain stable over a large number, ~4 × 10^6, of cycles at 100 Hz for the applied field, *i.e.*, for at least 12 hours.

The droplets segregate into two symmetric planes, both of which are not in contact with the electrodes. This is unexpected in a dielectric medium, because the metal electrode attracts the dipoles (as can be visualized by constructing image dipoles as in electrostatics). The reason for this separation is likely related to the fact that in a leaky dielectric medium, an electrical field gradient along the electric field direction arises due to the accumulation of ions near the electrode. Since the silicone oil droplets have a dielectric constant that is smaller than the medium, the (negative) dielectrophoretic (DEP) force that results from the electric field gradient would tend to repel the droplets from the substrate. This separation is a very useful feature for microlenses, as they are not limited to being plano-convex.

2D localization of droplet microlenses

The dielectrophoretic effect observed above suggests that one should be able to achieve in-plane absolute positioning of droplets as well. We demonstrate here that the droplets can be spatially localized in-plane into desired configurations. An example of droplet arrangement in a hexagonal lattice is shown in Fig. 5. For this purpose, one of the ITO electrodes was selectively etched by photo-lithography such that an array of roughly circular ITO-free regions (radius ~20 μm and spacing ~45 μm) is obtained. An emulsion of silicone oil and castor oil (ε_{ex} ~ 4.5, σ_{ex} ~ 7 × 10^{-10} S m^{-1}, η_{ex} ~ 0.8 Pa s) in a volume ratio of 1 : 16 is confined between the uniform ITO electrode and the etched ITO electrode with a periodic array of roughly circular holes. Upon switching the frequency from 3 Hz (Fig. 5a), where the droplet size distribution is polydisperse and droplet breakup events are frequent, to 8 Hz (Fig. 5b), where droplet coalescence events are more dominant, the droplets are driven to the circles due to negative dielectrophoresis (see Movie S1†). At ν = 40 Hz, where the electrohydrodynamic forces are weak relative to the dipolar

 This journal is © The Royal Society of Chemistry 2014

Published on 13 December 2013. Downloaded by Memorial University of Newfoundland on 22/06/2014 16:08:23.

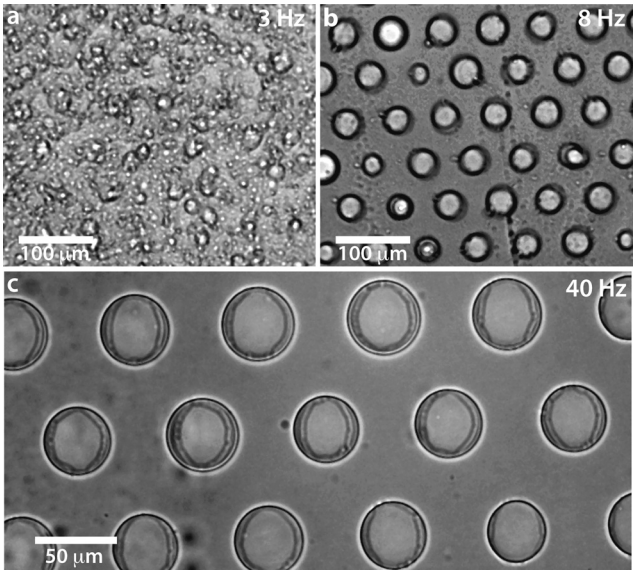

Fig. 5 In-plane localization *via* DEP. An emulsion of silicone oil drops in castor oil is confined between two ITO-on-glass electrodes: one uniform and one with a periodic array of circular holes etched out of the ITO. Upon increasing the frequency (ν) from (a) 3 Hz to (b) 8 Hz at E = 10 V μm^{-1}, roughly monodisperse droplets (b, 8 Hz) are obtained from a polydisperse (a, 3 Hz) distribution. The droplets are trapped by the circular holes due to negative dielectrophoresis. (c) Static silicone oil droplets are located on top of the roughly circular ITO-free regions when the electrohydrodynamic forces are weak relative to the dipolar forces at ν = 40 Hz (E = 10 V μm^{-1}).

forces, an array of droplets with radii close to (but slightly larger than) the size of the pattern (bottom) is obtained (Fig. 5c).

Conclusion

In summary, we have described a protocol to obtain both 2D and quasi-3D arrays of microlenses. The shape of the microlenses and thereby their focusing property is controlled by simply changing the frequency of the imposed electric field, *via* an electrohydrodynamic mechanism. We have achieved a large dynamic range of shape deformation from an oblate (lentil shaped) spheroid to a prolate (egg shaped) spheroid. The focal length change is observed to be about 35% and the numerical aperture (NA) changes from 0.18 to 0.24 going from large to small frequencies. We also demonstrate localization of the droplet microlenses in a two-dimensional hexagonal array. This study provides a starting point to generate more complex spatial arrangements of tunable microlenses.

Acknowledgements

We thank Ms. Bhagyashree Chalke and Mr. Pritesh Parikh for their help in fabrication of the square grid.

References

1 N.-T. Nguyen, *Biomicrofluidics*, 2010, **4**, 031501.
2 B. Berge and J. Peseux, *Eur. Phys. J. E: Soft Matter Biol. Phys.*, 2000, **3**, 159–163.
3 T. Krupenkin, S. Yang and P. Mach, *Appl. Phys. Lett.*, 2003, **82**, 316–318.
4 L. Dong, A. K. Agarwal, D. J. Beebe and H. Jiang, *Adv. Mater.*, 2007, **19**, 401–405.
5 L. Dong, A. K. Agarwal, D. J. Beebe and H. Jiang, *Nature*, 2006, **442**, 551–554.
6 P. Fei, Z. He, C. Zheng, T. Chen, Y. Men and Y. Huang, *Lab Chip*, 2011, **11**, 2835–2841.
7 N. Chronis, G. Liu, K.-H. Jeong and L. Lee, *Opt. Express*, 2003, **11**, 2370–2378.
8 D.-Y. Zhang, V. Lien, Y. Berdichevsky, J. Choi and Y.-H. Lo, *Appl. Phys. Lett.*, 2003, **82**, 3171–3172.
9 H. Ren and S.-T. Wu, *Opt. Express*, 2008, **16**, 2646–2652.
10 C.-C. Yang, C. G. Tsai and J. A. Yeh, *Biomicrofluidics*, 2010, **4**, 043006.
11 F. Mugele and J.-C. Baret, *J. Phys.: Condens. Matter*, 2005, **17**, R705–R774.
12 S. Yang, T. Krupenkin, P. Mach and E. Chandross, *Adv. Mater.*, 2003, **15**, 940–943.
13 D. R. Link, S. L. Anna, D. A. Weitz and H. A. Stone, *Phys. Rev. Lett.*, 2004, **92**, 054503.
14 H. Boukellal, S. Selimović, Y. Jia, G. Cristobal and S. Fraden, *Lab Chip*, 2009, **9**, 331–338.
15 T. Tanaami, S. Otsuki, N. Tomosada, Y. Kosugi, M. Shimizu and H. Ishida, *Appl. Opt.*, 2002, **41**, 4704–4708.
16 M. Castellano-Muoz, A. Wei Peng, F. T. Salles and A. J. Ricci, *Microsc. Microanal.*, 2012, **18**, 753–760.
17 A. Varshney, S. Ghosh, S. Bhattacharya and A. Yethiraj, *Sci. Rep.*, 2012, **2**, 738.
18 D. B. Murphy, *Fundamentals of Light Microscopy and Electronic Imaging*, Wiley, 1st edn, 2001.
19 W. J. Smith, *Modern optical engineering*, McGraw-Hill, 4th edn, 2008.
20 J. R. Melcher and G. I. Taylor, *Annu. Rev. Fluid Mech.*, 1969, **1**, 111–146.
21 D. A. Saville, *Annu. Rev. Fluid Mech.*, 1997, **29**, 27–64.
22 P. F. Salipante and P. M. Vlahovska, *Phys. Fluids*, 2010, **22**, 112110.
23 N. Bentenitis and S. Krause, *Langmuir*, 2005, **21**, 6194–6209.
24 S. Torza, R. G. Cox and S. G. Mason, *Philos. Trans. R. Soc., A*, 1971, **269**, 295–319.
25 R. S. Allan and S. G. Mason, *Proc. R. Soc. London, Ser. A*, 1962, **267**, 45–61.